ACS APPLIED MATERIALS & INTERFACES

Research Article

www.acsami.org

A Benzodithiophene-Based Novel Electron Transport Layer for a Highly Efficient Polymer Solar Cell

Hong Il Kim,[†] Thi Thu Trang Bui,[‡,§] Guan-Woo Kim,[†] Gyeongho Kang,[†] Won Suk Shin,*[,‡,§] and Taiho Park*[,†]

[†]Department of Chemical Engineering, Pohang University of Science and Technology, 77 Cheongam-Ro, Nam-Gu, Pohang, Gyeongbuk 790-784, Korea

[‡]Energy Materials Research Center, Korea Research Institute of Chemical Technology, 141 Gajeong-Ro, Yuseong-Gu, Daejeon, 305-600, Korea

[§]Department of Nanomaterials Science and Engineering, University of Science and Technology (UST), 217 Gajeong-Ro, Yuseong-Gu, Daejeon, 305-350, Korea

Supporting Information

ABSTRACT: We designed and synthesized a novel conjugated polyelectrolyte (CPE), poly{3-[2-[4,8-bis(2-ethylhexyloxy)-6-methyl-1,5-dithia-*s*-indacen-2-yl]-9-(3-dimethylamino-propyl)-7-methyl-9H-fluoren-9-yl]-propyl}-dimethylamine (PBN). We employed PBN as an electron-transporting layer on a ZnO layer and constructed a highly efficient, inverted structure device consisting of a mixture of poly({4,8-bis[(2-ethylhexyl)oxy]benzo[1,2-*b*:4,5-*b*′]dithiophene-2,6-diyl}{3-fluoro-2-[(2-ethylhexyl)carbonyl]thieno[3,4-*b*]-thiophenediyl}) (PTB7) and $PC_{70}BM$, achieving a high power conversion of up to 8.6%, constituting a 21.1% improvement over the control device performance (7.1%) prepared without a PBN layer. This result was ascribed to the reduced interfacial resistance and the improved charge transport and collection through the PBN electron transport layer.

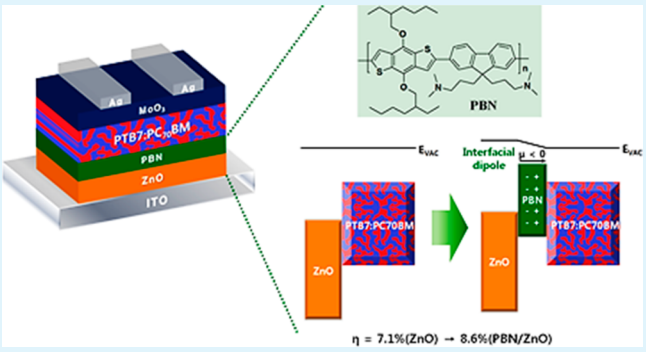

KEYWORDS: *polymer solar cell, electron transport layer, PBN, water-/alcohol-soluble polymers, conjugated polyelectrolyte*

INTRODUCTION

Polymer solar cells (PSCs) prepared with bulk-heterojunction (BHJ) formed using a mixture of electron donor polymers and electron acceptor fullerene derivatives (e.g., $PC_{60}BM$ and $PC_{70}BM$) are promising as alternatives to conventional silicon-based solar cells because the devices are prepared using materials that are readily processed, low in cost, and easily applied.[1−4] Numerous efforts have been devoted to improving power conversion efficiency (PCE), for instance, by developing new electron donor materials[5−10] or device architectures.[11−15] Alternatively, the PCE, especially in an inverted device, may be significantly improved by optimizing the interfaces between the electrodes and the active layers using a modified *n*-type metal oxide,[16−19] carbon nanotubes,[20] or self-assembled monolayers.[21−23] Kim et al. described the use of a water- and alcohol-soluble conjugated polyelectrolyte (CPE) polymer, poly(9,9′-bis(6″-*N*,*N*,*N*-trimethylammoniumhexyl)-fluorene-*co*-alt-phenylene) (FPQ) with bromide counterions, as an interlayer between TiO_x and the active layer to improve electron transport at the cathode and block hole transport to the cathode. This approach yielded a highly efficient PSC based on a poly(3-hexylthiophene) (P3HT):$PC_{60}BM$ system.[24] Wu et al.,[25] Gong et al.,[26] and Chang et al.[27] independently employed PFN as an interlayer between ZnO and an active layer and reported improvements in the PCEs of inverted devices prepared from naphtho[1,2-c:5,6-c]bis[1,2,5]thiadiazole-based polymers (PBDT-DTNT) (η increased from 6.1 to 8.4%) or poly({4,8-bis[(2-ethylhexyl)oxy]benzo[1,2-*b*:4,5-*b*′]-dithiophene-2,6-diyl}{3-fluoro-2-[(2-ethylhexyl) carbonyl]-thieno[3,4-*b*]thiophenediyl}) (PTB7) (η increased from 7.28 to 8.01%). These results suggested that the development of an appropriate interlayer could be as important as the development of new photoactive polymers for realizing PSCs with a high PCE.

Herein, we report the development of a novel CPE polymer (PBN) having a novel benzodithiophene (BDT)-based molecular structure (Figure 1). The coating of PBN on the ZnO layer to form a PBN/ZnO stacked structure improved the physical contact between the ZnO and PTB7:$PC_{70}BM$-based active layers and improved the wettability of a mixture of PTB7:$PC_{70}BM$ on the ZnO layer. The PBN/ZnO stacked

Received: May 30, 2014
Accepted: September 4, 2014
Published: September 4, 2014

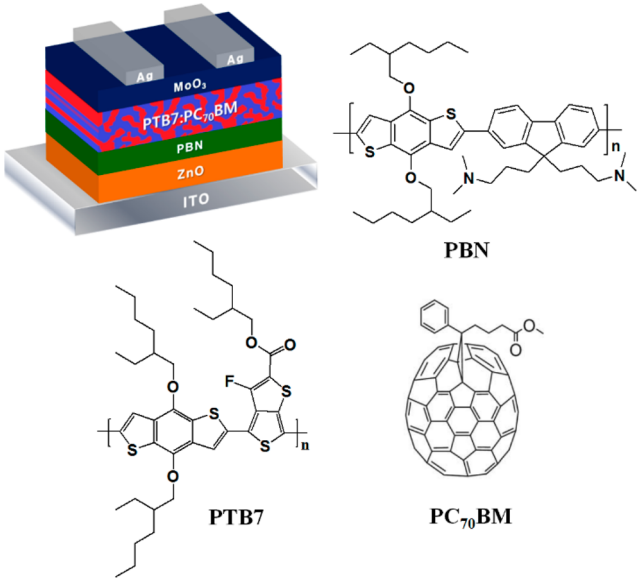

Figure 1. Schematic illustration of the device architectures of the inverted PSCs, and the molecular structures of PTB7, PBN, and $PC_{70}BM$.

structure reduced the interfacial energy barrier by generating an interfacial dipole moment between ZnO and the active layer.

The chemical structure of PBN is shown in Figure 1. The synthesis procedures are presented in Figure S1 (Supporting Information). The number-average molecular weight (M_n) of the synthesized PBN was determined using gel permeation chromatography (GPC) with polystyrene standards and chloroform as the eluent. A M_n of 13.1 kDa and a polydispersity index (PDI: M_w/M_n) of 1.34 were measured. The ultraviolet−visible (UV−vis) absorption spectrum of PBN is shown in Figure S2 (Supporting Information). The absorption maxima of PBN in solution and in the film state were observed at 464.0 or 463.5 nm, respectively. The optical band gap of PBN was determined from the UV−vis absorption onset of PBN in the film state. The PBN film displayed an optical band gap of 2.48 eV. The highest occupied molecular orbital (HOMO) and the lowest unoccupied molecular orbital (LUMO) energy levels of PBN were determined using cyclic voltammetry (CV), as shown in Figure S3 (Supporting Information). The HOMO and LUMO energy levels of PBN were observed at −5.16 and −2.66 eV, respectively.

RESULTS AND DISCUSSION

We optimized the PBN content in a ZnO layer in an inverted PSC. The optimal photovoltaic parameters are listed in Table 1 (also see Figure S4, Supporting Information). The control device prepared without an ETL (C1) yielded a PCE of 2.1% with a V_{OC} of 0.35 V, J_{SC} of 14.3 mA/cm^2, and FF of 42.1%. By introducing the ZnO layer (C2), the PCE increased to 7.1% with a V_{OC} of 0.73 V, J_{SC} of 13.6 mA/cm^2, and FF of 71.7%. These values agreed well with the results reported by Chang et al., who obtained a V_{OC} of 0.74 V, J_{SC} of 14.8 mA/cm^2, and FF of 66.5%, providing a 7.28% PCE using an inverted device structure.[27] The solvent effects of the interlayer were tested by fabricating the C3 device using methanol and acetic acid, without including PBN on the ZnO layer. The solvent-only (C2) device provided a lower efficiency than the C2 device. This result suggested that the small amount of acid affects the

Table 1. Summary of the Photovoltaic Parameters of the PTB7:$PC_{70}BM$-Based Devices Fabricated Using Different ETLs

devices	ETL	J_{SC} (mA/cm^2)	V_{OC} (V)	FF (%)	PCE (%)
C1	W/O	14.3	0.35	42.1	2.1
C2	ZnO	13.6	0.73	71.7	7.1
D0.005	0.005 w/v PBN	15.3	0.75	71.5	8.1
D0.01	0.01 w/v PBN	15.8	0.75	72.3	8.6
D0.02	0.02 w/v PBN	15.3	0.73	71.9	8.1
D0.04	0.04 w/v PBN	15.8	0.72	71.4	8.0
C3	Me−OH+CH_3COOH	13.2	0.75	69.2	6.8
C4	Ca	14.9	0.73	67.1	7.3

device performance. The presence of a PBN layer on the ZnO layer improved the photovoltaic performance (D0.005−D0.04) to an 8.0−8.6% PCE, indicating that the PBN layer provided better charge transport at the interface between the ZnO layer on ITO and the PTB7:$PC_{70}BM$ active layer in the devices. The best photovoltaic performance was obtained using 0.01 w/v PBN (D0.01), which enhanced the PCE to 8.6% with a J_{SC} of 15.8 mA/cm^2, V_{OC} of 0.75 V, and FF of 72.3%. Representative $J-V$ curves are presented in Figure 2. The PCE value was 21%

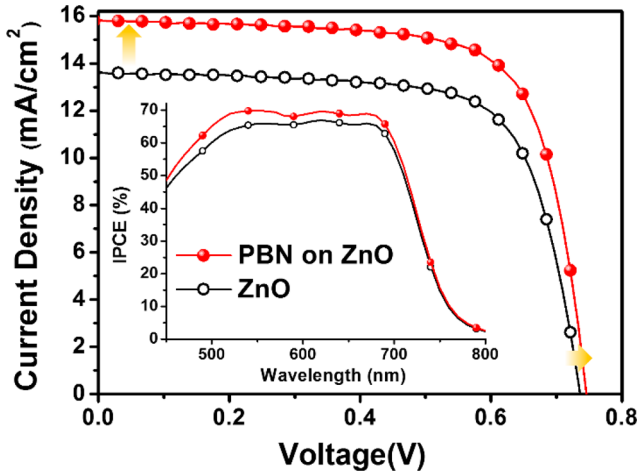

Figure 2. $J-V$ characteristics and IPCE spectra of PTB7:$PC_{70}BM$ on top of the ZnO and PBN/ZnO thin layers, respectively.

higher than that of the C2 device (7.1% PCE) having only a ZnO layer and 18% higher than that of the conventional device structure C4 (7.3% PCE). The improved photovoltaic performance of the device (D0.01) employing a PBN layer was mainly ascribed to the improvement in the J_{SC} values (from 13.6 (C2) to 15.8 mA/cm^2 (D0.01)), suggesting that the PBN layer reduced the interfacial energy barrier by tuning the interfacial dipole moment between the ZnO and active layers. Although there is no absorption spectra difference, PL quenching was increased by the employment of the PBN interlayer on the ZnO. So we can confirm that PBN/ZnO stacked structure improves an ability of charge transport than the bare ZnO layer (Figure S5,Supporting Information). Integrating the values of the measured incident photon to current conversion efficiency (IPCE) under AM 1.5 G illumination (100 mW/cm^2 solar spectrum) yielded J_{SC} values of 12.6 and 14.3 mA/cm^2 for the ZnO and PBN/ZnO devices, respectively (Figure 2 inset). These values were consistent with

the measured J_{SC} values of 13.6 and 15.8 mA/cm^2 for ZnO and PBN/ZnO, respectively, within an experimental error of ~9%.

The roles of PBN on the ZnO layer and the mechanism through which the PBN layer improved the photovoltaic performances of the inverted-type device were investigated by characterizing the morphology, surface energy, and dipole moments of the PBN layer on a ZnO layer, and the electrical properties of the devices were measured. The surface morphologies, obtained using scanning electron microscopy (SEM), confirmed the formation of a PBN film on top of the ZnO layer. A comparison of the image without and with a PBN layer on the surface of the ZnO layer clearly revealed that the PBN layer provided the coverage of the ZnO layer surface (Figure 3b). The nanoscale surface morphologies were

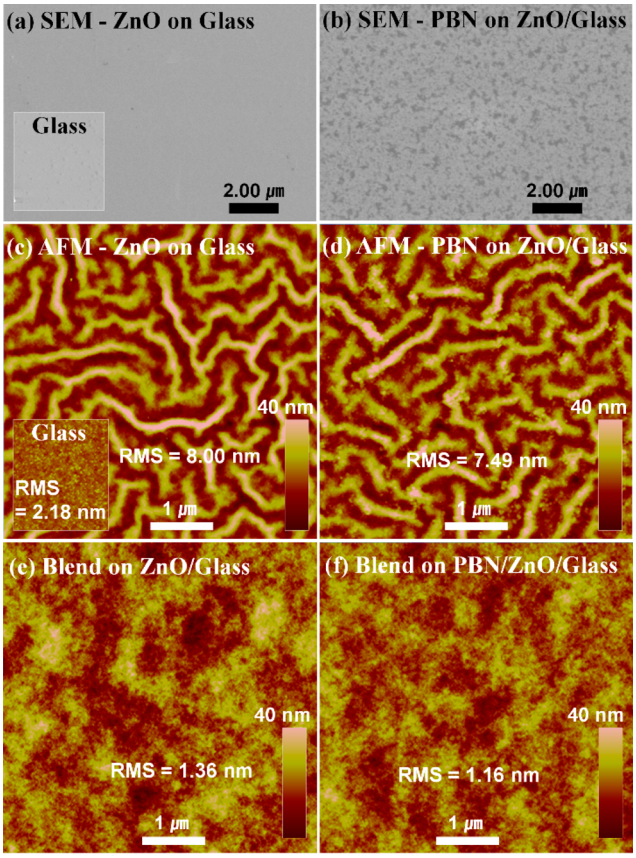

Figure 3. SEM images of (a) ZnO and (b) PBN/ZnO on top of glass, respectively. AFM tapping mode height images of (c) ZnO and (d) PBN/ZnO, respectively, and those of the PTB7:$PC_{70}BM$ blend on the (e) ZnO and (f) PBN/ZnO structures, respectively.

examined using tapping-mode atomic force microscopy (AFM). The root-mean-square (RMS) roughness of the ZnO layer and the PBN layer on a ZnO layer were 8.00 and 7.49 nm, respectively (Figure 3c,d), indicating that the ZnO surface was planarized by the PBN layer. The surface RMS roughness of the PTB7:$PC_{70}BM$ layer on the PBN layer was 1.16 nm, slightly smaller than the value (1.36 nm) measured on a ZnO layer alone (Figure 3e,f). The smooth surfaces of the PBN layer on the ZnO layer surface and the PTB7:$PC_{70}BM$ active layer on the PBN layer improved the compatibility between the ZnO layer and the active layer as well as between the active layer and the counter electrode, thereby improving contact. Improved contact was expected to increase charge transport at the interface between the ZnO layer and the PTB7:$PC_{70}BM$ active layer in the devices to provide a higher photovoltaic performance in devices (D0.01) prepared with a PBN layer on the ZnO surface layer.

Next, we measured the surface energies (γ_s) of the ZnO layer and of the layer after treatment with various amounts of PBN. The γ_s values are important for understanding the wettability and adhesion properties of an interface. We estimated γ_s using the Owens and Wedt geometric mean equation[28,29] commonly used to calculate the surface energy between two different liquids (e.g., water and glycerol). The water contact angles and surface energies are plotted in Figure 4 (see Figure S6,

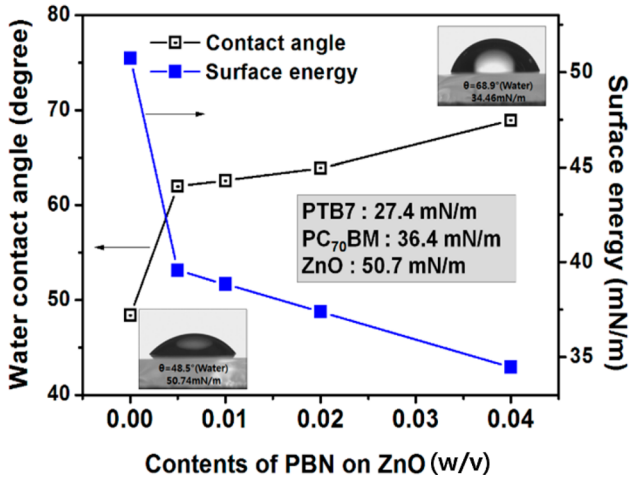

Figure 4. Water contact angles and surface energies of the ZnO and PBN/ZnO surfaces.

Supporting Information, for details). The introduction of PBN on the ZnO layer increased the water contact angle from 48.5° to 68.9°, indicating that the PBN/ZnO surface was more hydrophobic than the ZnO-only surface. The hydrophobic benzodithiophene units of the PBN were apparently organized at the air interface, whereas the hydrophilic quaternary amine units formed by the reaction with acetic acid appeared to be concentrated at the ZnO layer surface. These results suggested that the PBN layer introduced an interfacial dipole moment at the ZnO layer surface. In addition to increasing the hydrophobicity, the γ_s value of the ZnO layer surface decreased upon introduction of an additional PBN layer, from 50.74 to 34.46 mN/m. The value of γ_s for a PTB7:$PC_{70}BM$ blend (1:1.5 w/w) was measured to be 31.36 mN/m. The individual values of PTB7 and $PC_{70}BM$ were measured to be 27.4 and 36.4 mN/m, respectively (Figure S6, Supporting Information). The photoinduced electrons were easily transported and extracted from the active layer to the working electrode through the PBN interfacial layer. We maintained the humidity of 50% at 30 °C and tested the long-term stability of the devices for 200 h without encapsulation (Figure S7, Supporting Information). The stability of the PBN/ZnO cell may have been due to the hydrophobic properties of the electron transporting layer, which prevented oxidation and water penetration into the active layer surface.

Ultraviolet photoelectron spectroscopy (UPS) was used to characterize the dipole moment at the ZnO layer surface as a result of the PBN layer (Figure S8, Supporting Information). Figure 5 shows the kinetic energy differences of the ZnO layer before and after PBN treatment in the inelastic cutoff region.

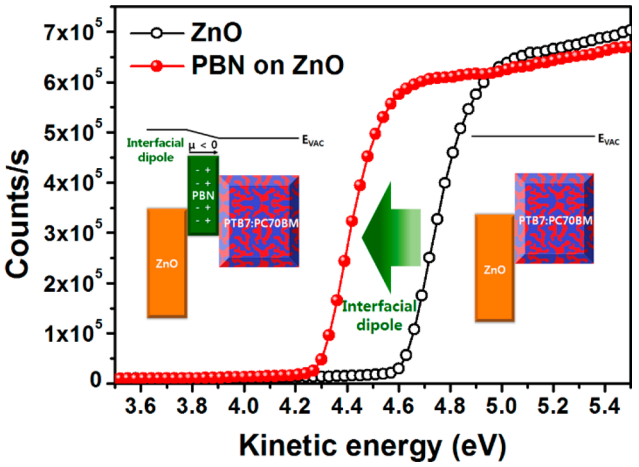

Figure 5. UPS spectra of the ZnO layer, before and after PBN treatment, in the inelastic cutoff region of the ZnO and PBN/ZnO thin layers. The schematic energy diagrams of the ZnO and the PBN/ZnO thin layers.

The cutoff energy (E_{cutoff}) was defined as the lowest kinetic energy of the measured electrons and provided an estimate for the work function (WF). The E_{cutoff} value of the ZnO layer after PBN treatment was 0.3 eV lower than that of the ZnO layer, indicating that the WF of the ZnO layer after PBN treatment was shifted by 0.3 eV toward the vacuum level, as illustrated in the insets of Figure 5. This indicated that the interfacial dipole moment generated between the electron transport layer and the active layer increased upon PBN treatment.

Figure 6a shows the dark $J-V$ characteristics of PTB7:$PC_{70}BM$ blends prepared on a ZnO layer prior to (C2) or after (D0.01) PBN treatment. The calculated series resistance (R_S), shunt resistance (R_{SH}), and rectification ratios are listed in Table 2. The R_S values were attributed to Ohmic loss in the device due to the resistance of the contacts between the active layer and the electrode, as well as to the parasitic probe resistance. The introduction of a PBN layer on the ZnO thin layer reduced RS for D0.01 from 2.54 to 1.37 Ωcm^2. This result provided an explanation for the observed improvement in J_{SC}, from 14.2 to 15.8 mA/cm^2 in D0.01. The R_{SH} values of C2 and D0.01 were 5.96×10^3 and 1.35×10^4 Ωcm^2, respectively, indicating that D0.01 prepared with the PBN layer had a lower leakage current and excellent diode characteristics with a higher rectification ratio. These effects improved the FF from 71.7 to 72.3%.

Table 2. Summary of the Electrical Parameters Measured from the ZnO and PBN/ZnO Inverted Devices

ETL	device	R_S (Ωcm^2)	R_{SH} (Ωcm^2)	rectification ratio	$\mu_{electron}$ [$cm^2/(V\ s)$]
ZnO[a]	C1	2.54	5960	2690	5.80×10^{-6}
PBN/ZnO[b]	D0.01	1.37	13 500	8750	1.80×10^{-5}

[a]ITO/ZnO/PTB7:$PC_{70}BM$/MoO_3/Ag. [b]ITO/ZnO/PBN/PTB7:$PC_{70}BM$/MoO_3/Ag.

Space charge limited current (SCLC) measurements were carried out in electron-only devices, and the charge carrier mobilities were calculated (Table 2). Figure 6b shows the dark $J-V$ characteristics of the electron-only devices. The electron mobility was estimated using the SCLC model[30,31] with the following diode structure Al/ETL/PTB7:$PC_{70}BM$/Al for the electron and was found to be $J = 9\varepsilon_0\varepsilon_r\mu V^2/8L^3$, where ε_0 is the permittivity of free space (8.85×10^{-12} $m^{-3}kg^{-1}s^4A^2$), ε_r is the dielectric constant of the polymer (3), μ is the hole mobility, V is the voltage drop across the device, and L is the polymer thickness (70 nm). The electron mobility of the PTB7:$PC_{70}BM$ blend on the ZnO layer after treatment with PBN was 1.80×10^{-5} $cm^2/(V\ s)$, significantly greater than the value (5.80×10^{-6} $cm^2/(V\ s)$) obtained from the ZnO-only layer. This result indicated that the introduction of a PBN layer on the ZnO surface improved the interfacial contact between the electron transport layer and the active layer, thereby enhancing the PCE in the PBN/ZnO-based devices, such as D0.01, to a PCE of 8.6%.

CONCLUSIONS

We designed and synthesized a novel BDT-based water- and alcohol-soluble conjugated polyelectrolyte (CPE) polymer, PBN, and demonstrated the fabrication of highly efficient, inverted PSC devices based on the use of a PBN/ZnO stacked structure as the electron transport layer. The introduction of PBN on the ZnO surface to yield a PBN/ZnO stacked structure became more hydrophobic and displayed a reduced surface energy, improving the wettability and physical contact between the ZnO and PTB7:$PC_{70}BM$-based active layer. The PBN/ZnO stacked structure reduced the energy barrier between the ZnO and $PC_{70}BM$ layers by increasing the interfacial dipole moment between the ZnO and

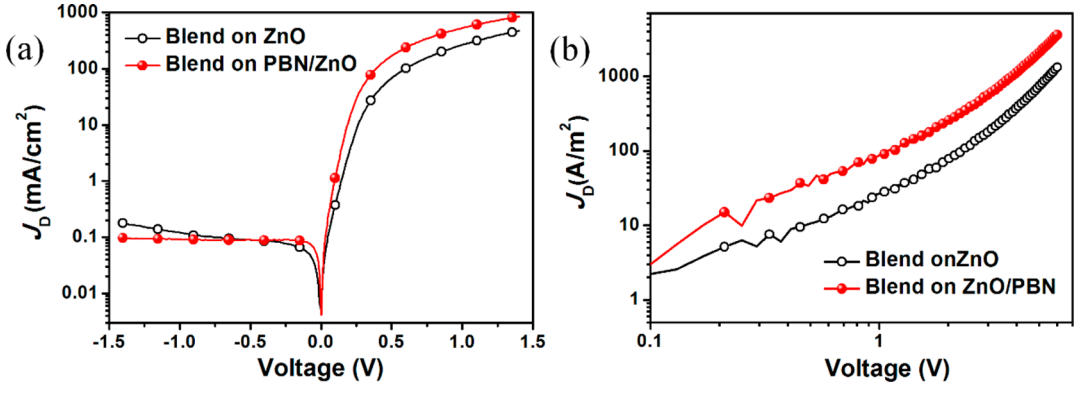

Figure 6. Measured dark $J-V$ characteristics of (a) the PTB7:$PC_{70}BM$ blend on the ZnO layer, and the PBN/ZnO architecture, respectively, and (b) the electron-only PTB7:$PC_{70}BM$ layer on ZnO or PBN/ZnO devices.

PTB7:$PC_{70}BM$-based active layers. Electron extraction and transport were thereby improved. The PBN layer improved the electron collection efficiency of the inverted devices and smoothed the ZnO surfaces, which improved the device performance and stability. The introduction of a PBN/ZnO electron transport layer improved the J_{SC} and FF and yielded a PCE of 8.6%, representing a 21.1% improvement over the control device. These results suggest a new strategy for developing efficient polymer solar cells. Further performance enhancements may potentially be realized by carefully tuning the structure of the water- and alcohol-soluble conjugated polyelectrolyte (CPE) polymer, PBN.

■ ASSOCIATED CONTENT

Supporting Information

Experimental details, UV−vis spectra, cyclic voltammogram, *J*−*V* characteristics, PL quenching data, contact angles, long-term stability test, and ultraviolet photoelectron spectroscopy spectra. This material is available free of charge via the Internet at http://pubs.acs.org.

■ AUTHOR INFORMATION

Corresponding Authors

*E-mail: shinws@krict.re.kr.
*E-mail: taihopark@postech.ac.kr.

Notes

The authors declare no competing financial interest.

■ ACKNOWLEDGMENTS

This work was supported by grants from the Center for Advanced Soft Electronics under the Global Frontier Research Program (2012M3A6A5055225), the Basic Science Research Program (No. 2011-0030343), and the Nano Material Technology Development Program (2012M3A7B4049989), through an NRF funded by the MSIP (Korea). This work was also supported by POSCO under contract number 2011Y107.

■ REFERENCES

(1) Li, G.; Zhu, R.; Yang, Y. Polymer Solar Cells. *Nat. Photonics* **2012**, *6*, 153−161.
(2) Andersen, T. R.; Dam, H. F.; Andreasen, B.; Hösel, M.; Madsen, M. V.; Gevorgyan, S. A.; Søndergaard, R. R.; Jørgensen, M.; Krebs, F. C. A Rational Method for Developing and Testing Stable Flexible Indium- and Vacuum-Free Multilayer Tandem Polymer Solar Cells Comprising Up to Twelve Roll Processed Layers. *Sol. Energy Mater. Sol. Cells* **2014**, *120*, 735−743.
(3) Galagan, Y.; Coenen, E. W. C.; Zimmermann, B.; Slooff, L. H.; Verhees, W. J. H.; Veenstra, S. C.; Kroon, J. M.; Jørgensen, M.; Krebs, F. C.; Andriessen, R. Scaling Up ITO-Free Solar Cells. *Adv. Energy Mater.* **2014**, *4*, 1300498.
(4) Espinosa, N.; Hösel, M.; Jørgensen, M.; Krebs, F. C. Large-Scale Deployment of Polymer Solar Cells on Land, on Sea, and in the Air. *Energy Environ. Sci.* **2014**, *7*, 855−866.
(5) Liang, Y.; Xu, Z.; Xia, J.; Tsai, S. T.; Wu, Y.; Li, G.; Ray, C.; Yu, L. For the Bright Future-Bulk Heterojunction Polymer Solar Cells with Power Conversion Efficiency of 7.4%. *Adv. Mater.* **2010**, *22*, E135−E138.
(6) Piliego, C.; Holcombe, T. W.; Douglas, J. D.; Woo, C. H.; Beaujuge, P. M.; Frechet, J. M. Synthetic Control of Structural Order in *N*-Alkylthieno[3,4-c]pyrrole-4,6-dione-Based Polymers for Efficient Solar Cells. *J. Am. Chem. Soc.* **2010**, *132*, 7595−7597.
(7) Carsten, B.; Szarko, J. M.; Son, H. J.; Wang, W.; Lu, L.; He, F.; Rolczynski, B. S.; Lou, S. J.; Chen, L. X.; Yu, L. Examining the Effect of the Dipole Moment on Charge Separation in Donor-Acceptor Polymers for Organic Photovoltaic Applications. *J. Am. Chem. Soc.* **2011**, *133*, 20468−20475.
(8) Najari, A.; Beaupré, S.; Berrouard, P.; Zou, Y.; Pouliot, J.-R.; Lepage-Pérusse, C.; Leclerc, M. Synthesis and Characterization of New Thieno[3,4-*c*]pyrrole-4,6-dione Derivatives for Photovoltaic Applications. *Adv. Funct. Mater.* **2011**, *21*, 718−728.
(9) Dou, L.; Chen, C.-C.; Yoshimura, K.; Ohya, K.; Chang, W.-H.; Gao, J.; Liu, Y.; Richard, E.; Yang, Y. Synthesis of 5H-Dithieno[3,2-*b*:2′,3′-*d*]pyran as an Electron-Rich Building Block for Donor−Acceptor Type Low-Bandgap Polymers. *Macromolecules* **2013**, *46*, 3384−3390.
(10) Liu, Y.; Chen, C. C.; Hong, Z.; Gao, J.; Yang, Y. M.; Zhou, H.; Dou, L.; Li, G.; Yang, Y. Solution-Processed Small-Molecule Solar Cells: Breaking the 10% Power Conversion Efficiency. *Sci. Rep.* **2013**, *3*, 3356.
(11) Kim, J. Y.; Lee, K.; Coates, N. E.; Moses, D.; Nguyen, T. Q.; Dante, M.; Heeger, A. J. Efficient Tandem Polymer Solar Cells Fabricated by All-Solution Processing. *Science* **2007**, *317*, 222−225.
(12) Ameri, T.; Dennler, G.; Lungenschmied, C.; Brabec, C. J. Organic Tandem Solar Cells: A Review. *Energy Environ. Sci.* **2009**, *2*, 347−363.
(13) Dou, L.; You, J.; Yang, J.; Chen, C.-C.; He, Y.; Murase, S.; Moriarty, T.; Emery, K.; Li, G.; Yang, Y. Tandem Polymer Solar Cells Featuring a Spectrally Matched Low-Bandgap Polymer. *Nat. Photonics* **2012**, *6*, 180−185.
(14) You, J.; Dou, L.; Yoshimura, K.; Kato, T.; Ohya, K.; Moriarty, T.; Emery, K.; Chen, C. C.; Gao, J.; Li, G.; Yang, Y. A Polymer Tandem Solar Cell with 10.6% Power Conversion Efficiency. *Nat. Commun.* **2013**, *4*, 1445−1446.
(15) Chen, C.-C.; Dou, L.; Gao, J.; Chang, W.-H.; Li, G.; Yang, Y. High-Performance Semi-Transparent Polymer Solar Cells Possessing Tandem Structures. *Energy Environ. Sci.* **2013**, *6*, 2714−2720.
(16) Yip, H.-L.; Hau, S. K.; Baek, N. S.; Ma, H.; Jen, A. K. Y. Polymer Solar Cells That Use Self-Assembled-Monolayer- Modified ZnO/Metals as Cathodes. *Adv. Mater.* **2008**, *20*, 2376−2382.
(17) Small, C. E.; Chen, S.; Subbiah, J.; Amb, C. M.; Tsang, S.-W.; Lai, T.-H.; Reynolds, J. R.; So, F. High-Efficiency Inverted Dithienogermole−Thienopyrrolodione-Based Polymer Solar Cells. *Nat. Photonics* **2011**, *6*, 115−120.
(18) Song, C. E.; Ryu, K. Y.; Hong, S. J.; Bathula, C.; Lee, S. K.; Shin, W. S.; Lee, J. C.; Choi, S. K.; Kim, J. H.; Moon, S. J. Enhanced Performance in Inverted Polymer Solar Cells with D-π-A-Type Molecular Dye Incorporated on ZnO Buffer Layer. *ChemSusChem* **2013**, *6*, 1445−1454.
(19) Thambidurai, M.; Kim, J. Y.; Song, J.; Ko, Y.; Song, H.-j.; Kang, C.-m.; Muthukumarasamy, N.; Velauthapillai, D.; Lee, C. High Performance Inverted Organic Solar Cells with Solution Processed Ga-Doped ZnO as an Interfacial Electron Transport Layer. *J. Mater. Chem. C* **2013**, *1*, 8161−8166.
(20) Lee, J. M.; Park, J. S.; Lee, S. H.; Kim, H.; Yoo, S.; Kim, S. O. Selective Electron- or Hole-Transport Enhancement in Bulk-Heterojunction Organic Solar Cells with N- or B-Doped Carbon Nanotubes. *Adv. Mater.* **2011**, *23*, 629−633.
(21) Yip, H.-L.; Jen, A. K. Y. Recent Advances in Solution-Processed Interfacial Materials for Efficient and Stable Polymer Solar Cells. *Energy Environ. Sci.* **2012**, *5*, 5994−6011.
(22) O'Malley, K. M.; Li, C.-Z.; Yip, H.-L.; Jen, A. K. Y. Enhanced Open-Circuit Voltage in High Performance Polymer/Fullerene Bulk-Heterojunction Solar Cells by Cathode Modification with a C_{60} Surfactant. *Adv. Energy Mater.* **2012**, *2*, 82−86.
(23) Duan, C.; Zhong, C.; Liu, C.; Huang, F.; Cao, Y. Highly Efficient Inverted Polymer Solar Cells Based on an Alcohol Soluble Fullerene Derivative Interfacial Modification Material. *Chem. Mater.* **2012**, *24*, 1682−1689.
(24) Choi, H.; Park, J. S.; Jeong, E.; Kim, G. H.; Lee, B. R.; Kim, S. O.; Song, M. H.; Woo, H. Y.; Kim, J. Y. Combination of Titanium Oxide and a Conjugated Polyelectrolyte for High-Performance Inverted-Type Organic Optoelectronic Devices. *Adv. Mater.* **2011**, *23*, 2759−2763.

(25) He, Z.; Zhong, C.; Su, S.; Xu, M.; Wu, H.; Cao, Y. Enhanced Power-Conversion Efficiency in Polymer Solar Cells Using an Inverted Device Structure. *Nat. Photonics* **2012**, *6*, 593−597.
(26) Yang, T.; Wang, M.; Duan, C.; Hu, X.; Huang, L.; Peng, J.; Huang, F.; Gong, X. Inverted Polymer Solar Cells with 8.4% Efficiency by Conjugated Polyelectrolyte. *Energy Environ. Sci.* **2012**, *5*, 8208−8214.
(27) Chang, Y.-M.; Leu, C.-Y. Conjugated Polyelectrolyte and Zinc Oxide Stacked Structure as an Interlayer in Highly Efficient and Stable Organic Photovoltaic Cells. *J. Mater. Chem. A* **2013**, *1*, 6446−6451.
(28) Moon, B. J.; Lee, G. Y.; Im, M. J.; Song, S.; Park, T. In Situ Modulation of the Vertical Distribution in a Blend of P3HT and $PC_{60}BM$ via the Addition of a Composition Gradient Inducer. *Nanoscale* **2014**, *6*, 2440−2446.
(29) Owens, D. K.; Wendt, R. C. Estimation of the Surface Free Energy of Polymers. *J. Appl. Polym. Sci.* **1969**, *13*, 1741−1747.
(30) Kim, J.; Kwon, Y. S.; Shin, W. S.; Moon, S.-J.; Park, T. Carbazole-Based Copolymers: Effects of Conjugation Breaks and Steric Hindrance. *Macromolecules* **2011**, *44*, 1909−1919.
(31) Cha, H.; Lee, G. Y.; Fu, Y.; Kim, Y. J.; Park, C. E.; Park, T. Simultaneously Grasping and Self-Organizing Photoactive Polymers for Highly Reproducible Organic Solar Cells with Improved Efficiency. *Adv. Energy Mater.* **2013**, *3*, 1018−1024.